# On one imperfection estimation method for thin shell buckling in the design code RCC-MR

Ashok Kumar[1] Anindya Chatterjee[2]

[1]Indira Gandhi Center of Atomic Research, Kalpakkam, India TN, India
[2]Indian Institute of Technology, Kanpur, UP, India

This draft: August 5, 2018

**Abstract**

The shell design code RCC-MR is used for design of fast breeder reactor components operating at high temperatures. Thin shells from such applications can be designed against buckling using linear elastic buckling analysis, following procedures given in RCC-MR. Due to human safety considerations, detailed examination of such procedures are of interest to the broad scientific community. Among such procedures, in particular, RCC-MR provides a sequence of three alternative methods to quantify an imperfection value; and that imperfection value is used in subsequent design calculations specified in the code. Of these three methods, the third and last one seems potentially nonconservative. Here we critique that third method only, using some detailed numerical examples. These examples have been chosen with care, to demonstrate cause for concern in the method suggested by the code, and constitute the main contribution of this paper. The first example is a nonuniform cylindrical shell closed with a spherical endcap and subjected to external pressure. The second example is an ellipsoidal head joined to a cylinder and subjected to internal pressure. The third example is a shell that is shaped like an L-shaped pipe, under twisting and bending by an end load. In all three cases, the new computed imperfection quantity is found to be very small compared to the actual value used for computations (25 times smaller, in one case), and in two cases the result is quite insensitive to the actual imperfection used. We explain how the three different examples have managed to "trick" the imperfection quantification method in three different ways. We suggest that this imperfection quantification method in RCC-MR should be re-examined. The primary value of our paper is not in new thin-shell mechanics, but rather in identifying unexpected ways in which a particular step in thin shell design in a well known code might lead to dangerous designs in some cases.

## 1 Introduction

Commercial sodium-cooled fast rectors are typically designed to operate for more than 40 years. Factors like high temperature damage through creep-fatigue, frequent thermal transients, low operating pressure, cost reduction efforts, and manufacturing difficulties, all together lead to large and thin reactor assembly components. Engineering design of such structures, specifically against buckling, must consider many factors including lowered yield stress at high operating temperatures, large radius to thickness ratios, and the well known sensitivity to geometric imperfections in such thin shells. Codes that govern the design of such structures must be examined widely within the general scientific community, even a remote possibility of nonconservative designs has profound implications for human safety.

The French code RCC-MR (2012) is used predominantly to design shell structures against buckling at high temperatures. It is the most important code available for buckling design of structures operating at high temperatures (from 20°C to 700°C). For example, the ASME Section VIII Div-2 provides design rules

for operating temperature limited to 480°C. Thus, the importance of RCC-MR for structural design in the nuclear industry is great.

RCC-MR prescribes, among other things, how geometrical imperfection and yield stress can be used to compute reduction or knock-down factors on computed linear elastic buckling loads to ensure safety. Specifically, RCC-MR appendix A7 provides detailed procedures for calculating the safe buckling loads of thin shells, accounting for both plasticity and imperfection, through purely elastic analysis [1]. The background formulation and experimental validation of the buckling design procedure given in RCC-MR is readily available [2].

The research literature on shell buckling is vast. We note classical experimental and theoretical works as in [3], [4] and [5], but note also that matters are not fully settled and new studies with new loads, analyses, and experiments keep appearing, e.g., [6], [7], [8], and [9]. Given the great complexity of the set of all possible shell geometries, loads, and resulting behaviors, a design code allows a structural designer to proceed with relatively less detailed effort and greater confidence at the same time, provided the designer follows certain simplified procedures and checks that are laid down in the code.

We emphasize that the design code offers multiple approaches to a designer, and the designer is free to adopt any of them. For this reason, although alternative design procedures based on elasto-plastic analysis are available as well, they are not relevant to the present paper. Here we focus on those parts of the code that deal with elastic analysis based design. Such design is indeed carried out in the nuclear industry.

Geometric imperfection is a *critical* parameter in safe buckling load calculation. RCC-MR specifies three different methods to quantify imperfection from manufacturing tolerances. We will duly describe all three methods, which require some technical details, a little later in the paper. Any one of these imperfection estimates can, in principle, be used to calculate a safe buckling load. The imperfection estimates from the first two methods result in safe buckling loads, to the best of our knowledge, and have been validated against experiments [2]. The third method for imperfection quantification, which is potentially the least conservative, is the one we examine in this paper.

A human aspect of the design activity should be noted. RCC-MR provides several alternative methods of safe design, and the human designer has a design in mind and checks it against each of these methods until *one* method certifies the design as safe. For this reason, borderline unsafe designs are highly likely to *seek out* less-conservative design processes in the code. A shell designer in the nuclear industry often works under stringent operational requirements, cost constraints, material limitations, etc. Any procedure within the code which allows a designer to certify a borderline design as safe is therefore extremely attractive. Such a procedure offers both a way forward as well as moral absolution. It is not in the self-interest of a beleaguered designer to go above and beyond the code. For these reasons, even a small source of rare risks in nuclear reactor shell design demands attention from the scientific research community.

With the above motivation, the aim of this paper is to critique the third method of imperfection quantification allowed by RCC-MR. We do emphasize that in general RCC-MR is comprehensive and impressive, and forms the mainstay of many design procedures in the nuclear industry of some countries including India. Our understanding of the specific calculation we critique below was gained fortuitously through other work not reported here, and we continue to hold RCC-MR in high regard in spite of it.

In this paper, we will present detailed buckling design calculations for three example structures following the abovementioned (third) calculation alternative as specified in RCC-MR. We have chosen these structures with some care, to illustrate ways in which the imperfection estimation can lead to potentially highly nonconservative designs. Our concluding suggestion will be that this third method should be re-examined, if not removed entirely.

## 2 Safe buckling load as per RCC-MR-A7

For completeness, we summarize the calculations prescribed by the code.

*RCC-MR, Section III, Tome 1, Subsection Z, technical appendix A7* is referred to below simply as RCC-MR-A7. RCC-MR-A7 provides reduction or knock-down factors for linear eigenvalue based buckling loads to account for geometrical imperfections and plasticity in real structures. We emphasize that the procedures we use here are based on elastic analysis. Design work in the nuclear industry is frequently based on purely elastic analysis based on RCC-MR, such as we examine here. RCC-MR does also discuss alternative elasto-plastic design approaches as well, but they are independent of the elastic analyses and do not affect the present paper.

### 2.1 Calculation procedure

To calculate the safe design buckling load of a structure, a linear elastic stress analysis and buckling analysis must first be carried out. This is routine linear finite element analysis with an arbitrarily chosen notional load $N$ (say, 1 KN or 1 MPa, as the case may be). Stresses in the structure due to this load are computed in the first step. In the second step, an elastic buckling load is computed using the so-called *eigenvalue analysis* to obtain a load multiplying factor, say $\lambda$; if $\lambda = 10.5$, for example, then buckling is predicted to occur at 10.5 times the notional load $N$ (i.e., at 10.5 KN if the notional load was 1 KN).

After the stress analysis of the first step, stresses obtained at critical locations in the shell are to be decomposed into membrane (mean) and bending (linearly varying) parts. This straightforward procedure is described further in appendix A1. Note that longitudinal and circumferential stresses are combined, and converted to von Mises stresses to quantify severity.

Subsequently, stresses are categorized into primary and secondary stresses as follows. (i) All membrane stresses are primary stresses. (ii) At locations far from geometrical discontinuities such as sudden changes in curvature, bending stresses are primary stresses as well. (iii) At or near geometrical discontinuities, bending stresses may be treated as secondary stresses[1].

After classifying the stresses obtained through finite element analysis (FEA) into primary and secondary stresses, we are allowed to drop secondary stresses from further consideration[2], except for the third method of imperfection quantification as mentioned below in due course.

The largest (von Mises) stress intensity obtained above is to be multiplied by the $\lambda$ obtained from eigenvalue analysis, giving a critical elastic stress. This stress is to be divided by the yield stress of the material, to obtain a non-dimensional number $\zeta$. Small $\zeta$ suggests that the structure's buckling response is elastic; large $\zeta$ implies plasticity will precede or accompany buckling.

Having computed $\zeta$ as above, we turn to geometrical imperfections, which the code allows us to quantify by three different methods, presented below in order of decreasing conservatism.

In the first method, the maximum deviation $d$ between the real and nominal shell geometry, measured normal to the nominal shell surface, is to be divided by shell thickness $h$ to obtain

$$\delta = d/h. \tag{1}$$

Larger $\delta$ leads to larger knock-down factors, as will be discussed in due course.

For the second method, the code says that sometimes

> "... it is possible only to consider a fraction of the previous value if it can be shown that the neglected fraction of the tolerance has no effect on instability. Thus, for a tube subjected to external pressure, only the ovalization tolerance is to be considered for defining the defect, to the exclusion of the mean diameter tolerance."

[1] See RCC-MR, Section III, Tome 1, Subsection B, table RB 3324.31 (pp. 97).

[2] The rationale is that secondary stresses can be relieved by local yielding without compromising the entire structure.

We have no further comment on the above two methods of quantifying imperfection. The third method of quantifying imperfection, potentially the least conservative, and also the one we critique in this paper, is as follows. The designer is allowed to define a new defect value $d_{new}$, which requires an additional linear elastic stress analysis of a deformed geometry generated by superimposing a scaled first buckling mode displacement on the nominal or perfect geometry. The scale factor is chosen to match the actual geometrical defect magnitude. From this additional analysis, the maximum stress intensity $S_d$ (membrane plus bending, *not* dropping secondary stresses) is used to calculate

$$d_{new} = \frac{h}{6}\left(\frac{S_d}{P_m} - 1\right), \tag{2}$$

where $P_m$ is the maximum membrane stress from the linear analysis, and $h$ is the shell thickness. We adopt the smaller of the two $P_m$'s, from the ideal and the perturbed geometries, as a conservative step. Subsequently, the designer takes

$$\delta = \frac{d_{new}}{h},$$

which could potentially be nonconservative if $d_{new} \ll d$.

General readers may note that quantification of imperfection plays a *critical* role in the thin shell design process, which is conducted under various constraints as described earlier. The pressure on the designer to produce a thin-walled yet safe design is high. Keeping imperfection low has practical difficulties. For example, in a shell of diameter 14 m and thickness 21 mm, a radial imperfection of 14 mm represents merely 0.1% of the diameter, yet gives $\delta = 2/3$ (recall Eq. 1), usually too large for the resulting design to be practical. In such circumstances, a code-backed method of computing a smaller effective imperfection may seem like a blessing. For this reason, critical examination of this third method of imperfection estimation is important.

With $\zeta$ and $\delta$ computed as above, the reduction factor $X(\zeta, \delta)$ is found from two charts provided in the code: one for stable and one for unstable post-buckling behaviors. Figure 1 shows the chart for unstable post-buckling, adapted from RCC-MR.

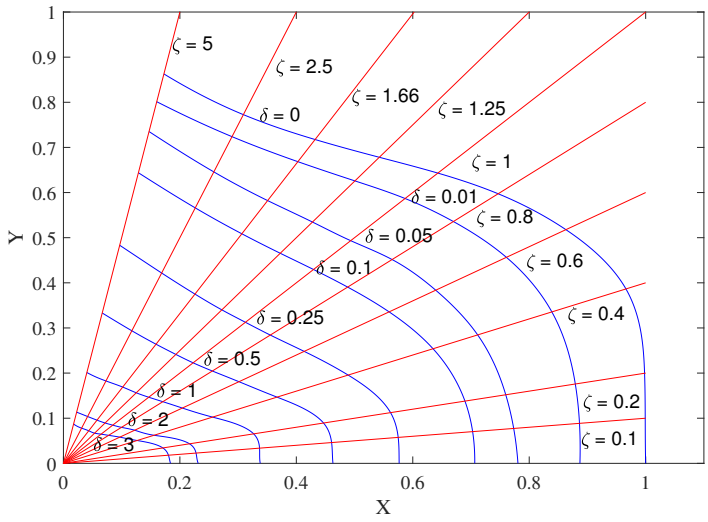


Figure 1: RCC-MR reduction factor chart for unstable post-buckling behavior. $X$ is as in Eq. 3, and $Y = \zeta X$. We have extracted the data and developed an interpolation program (details omitted), so arbitrary numerical values can be used.

Finally, the safe load for the structure is specified as the original load times the load multiplying factor

times $X(\zeta, \delta)$, divided by a further safety factor of 2.5, i.e.,

$$\text{Safe load} = \frac{(\text{Notional load } N) \times (\lambda \text{ from eigenvalue analysis}) \times X(\zeta, \delta)}{2.5}. \tag{3}$$

In the above, if the critical elastic stress value was not purely a membrane stress, but included both a membrane and a bending stress, then the safety factor would be 1.667 instead of 2.5.

From figure 1, for $X$ to be close to unity, one needs *both* (i) very low imperfection or small $\delta$, and (ii) predominantly elastic response at buckling, or small $\zeta$. These conditions may be practically impossible to achieve for (i) large thin walled structures (small $h$ increases $\delta$) (ii) operating at high temperatures (lowered yield strength raises $\zeta$). If a designer is forced to use $\delta = 1$, then the allowed stress levels may be too low to be useful: structural design may be unfeasible if one cannot exceed even 10% of yield stress. Yet, with other parameters held constant, if the code allows the designer to claim $\delta = 0.25$, then the allowed stress may double, making progress feasible.

We hope that a general reader will by now be convinced that use of Eq. 2 for nuclear reactor shell design potentially has very significant consequences.

# 3 Shell design case studies

In this paper we present case studies of three shell geometries, chosen so as to emphasize potential difficulties with Eq. 2.

First we note that RCC-MR-A7 provide reduction factors charts for un-stiffened shells, made of stainless steel 316 LN, whose properties are given in properties group A3.1S of [10]. The maximum value of $\zeta$ as defined in section 2, for which reduction factors are provided, is 5. Hence, dimensions and thickness of our shell examples below are chosen such that $\zeta$ remains below 5. Operating temperatures for these shells are taken notionally to be 20 degrees Centigrade; but it will be seen that the precise temperature is irrelevant. The Young's modulus and yield stress of the material, in our example calculations below, are taken to be 200 GPa and 220 MPa respectively; and Poisson's ratio is taken to be 0.3 (see [10]). No other material parameters are needed by the code. For our finite element calculations, the thin shell geometry is modeled in ABAQUS using first order, reduced integration, S4R elements.

In the following three subsections, we describe our three example shell structures. Analyses for these structures will be presented subsequently.

## 3.1 Example 1: Nonuniform cylinder with a spherical cap

See figure 2. We consider an axisymmetric thin shell, consisting of two concentric cylinders of different radii and heights, joined through two transition regions of large radii and a small conical region. The radius and height of the bottom cylinder are 2.3 m and 2.5 m respectively. The radius and height of the top cylinder are 1.15 m and 1.25 m respectively. The top edge of the upper cylinder is closed with a spherical cap of radius 3 m. The spherical cap and top cylinder are joined by a small fillet of radius 100 mm or 0.1 m. The wall thickness everywhere is 5 mm. The displacements of the bottom edge of the structure are arrested, as shown.

The spherical cap is subjected to external pressure of magnitude 50 KPa, as indicated schematically. A typical element size used in the calculation is of 20 mm, selected from mesh convergence studies (see appendix A2).

## 3.2 Example 2: Ellipsoidal head

See figure 3. We consider a structure composed of an axisymmetric ellipsoidal head on a cylindrical shell. In the cross section shown in figure 3 (left), the elliptical curve represents the head; the aspect ratio of

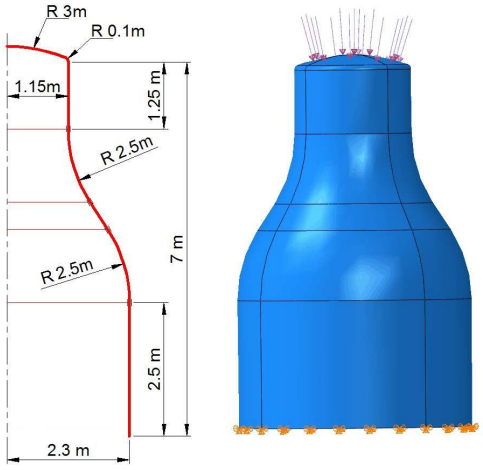


Figure 2: A nonuniform cylinder with a spherical cap. Left: schematic diagram with dimensions. Right: ABAQUS model with loading and boundary conditions.

the quarter-ellipse shown in the cross section is 4. The radius of the cylindrical shell is 4 m. All shell wall thicknesses are 2.5 mm. All displacement degrees of freedom of the top edge of the cylinder are arrested, as shown in the figure (right). The entire structure is subjected to an internal pressure of 15 KPa. Based on mesh convergence studies (see appendix A2), an element size of 25 mm is used.

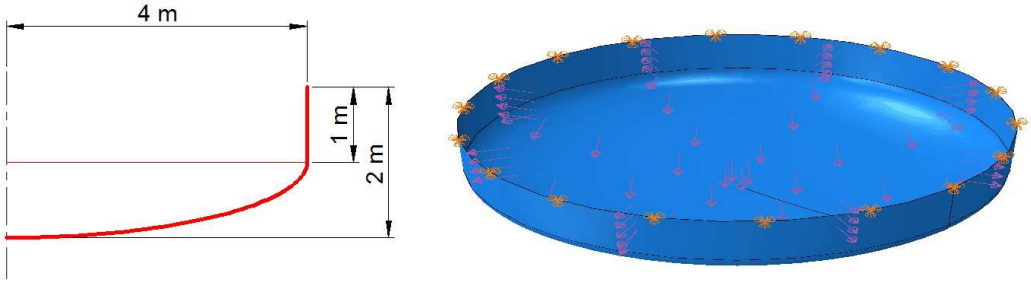


Figure 3: Ellipsoidal head. Left: schematic diagram with dimensions. Right: ABAQUS model with loading and boundary conditions.

### 3.3 Example 3: L-shaped shell under vertical end load

See figure 4. We consider a thin shell consisting of two cylinders of radius 1 m and length 10 m, perpendicular to each other, with an elbow shaped connection between them. The radius of the elbow's centerline is 3 m. The shell geometry is generated by sweeping a circle (figure, left) along a curve (figure, middle). The shell thickness is 5 mm. One end of the shell is assigned a built-in boundary condition (all dofs restrained), and the other end is subjected to a vertically downward distributed force (figure, right), of magnitude 1000 N/m. Based on mesh convergence studies (see appendix A2), an element length of 50 mm is used.

## 4 Imperfection quantification

The three shells given in subsections 3.1, 3.2 and 3.3 do not, in our opinion, involve extreme or outlandish geometries. They represent reasonable design situations. We now work out how a designer following the

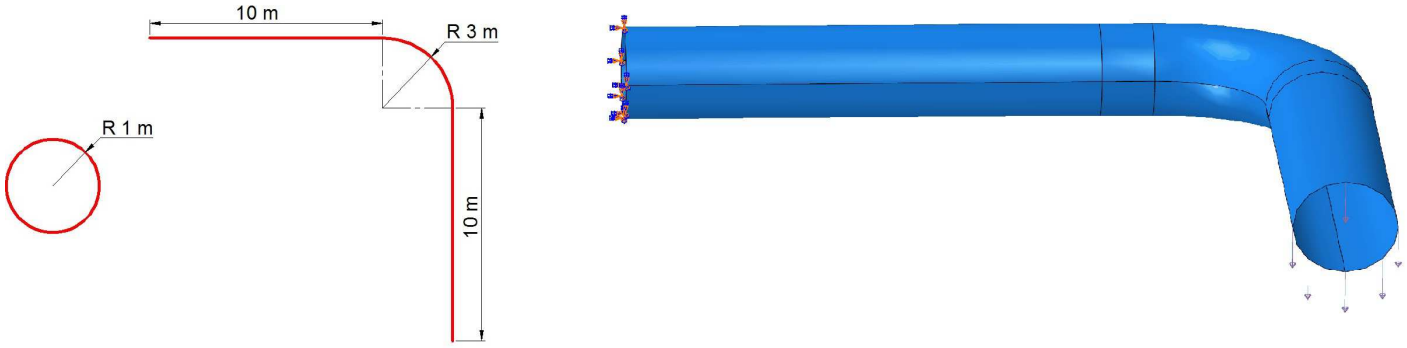


Figure 4: L-shaped shell. Left: circular cross section. Middle: swept path used to define geometry. Right: boundary conditions and downward-acting end loads.

code might estimate the safe loads for these shell structures.

For each of the three shells, we will proceed as follows. Recall section 2 and Eq. 2. $S_d$ is the maximum stress intensity (bending plus membrane), while $P_m$ is the largest membrane stress. To be conservative, we interpret $S_d$ to be the largest value obtained in the geometrically perturbed structure, and take $P_m$ to be the smaller among the two largest values (unperturbed and perturbed geometries).

## 4.1 Nonuniform cylinder with a spherical cap

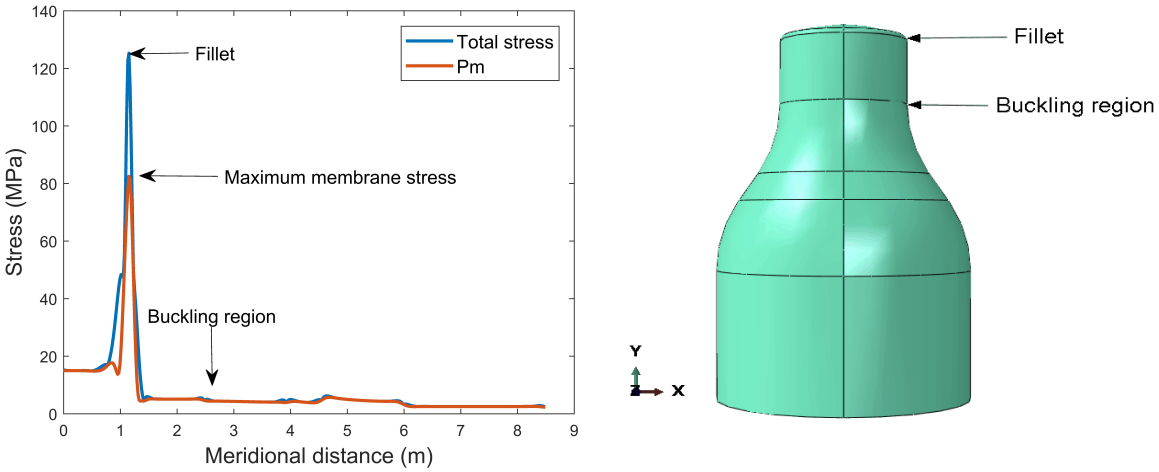


Figure 5: Left: membrane stresses, and total stresses (von Mises), plotted against curvilinear distance along the shell. Right: some key locations on the shell.

First, analysis results for the ideal structure are presented in figure 5. The key property of this structure, for our purposes, is that the buckling region is removed from the region of most severe stresses. Figure 5 shows stress plots on the left, and the structure on the right, with two locations marked: fillet region and buckling region. The largest bending stress and the largest membrane stress both occur at the fillet, far from the buckling region. Since the most severe stress occurs near a point of discontinuity in the geometry, the bending stress there is treated as a secondary stress (recall section 2). Results from the linear eigenvalue analysis are shown in figure 6, and show the buckled shape (with displacements exaggerated).

Now, as per the recommendation leading to Eq. 2, we are supposed to perturb the shell geometry in

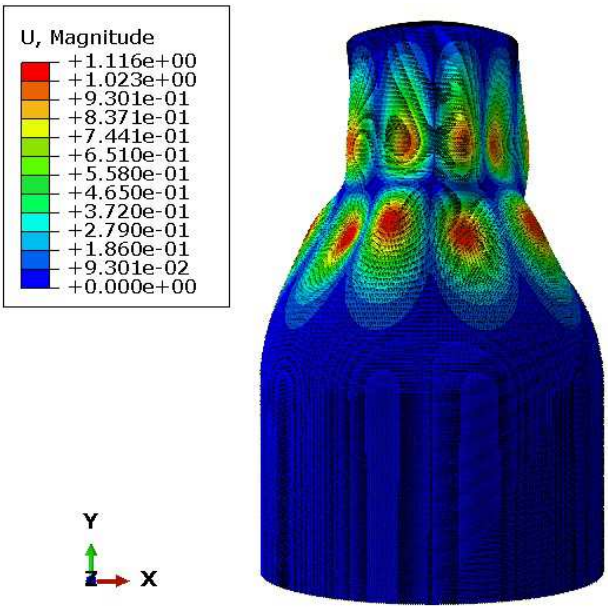


Figure 6: First linear elastic buckling mode of nonuniform cylinder with spherical cap. Displacements are exaggerated.

the same shape as the buckling mode, but with an amplitude equal to the imperfection present (or, in the case of designs, the imperfection allowed). It is a practical fact that no thin shell designer in the nuclear industry can assume an imperfection higher than the shell thickness, or $d/h > 1$ (recall the discussion following figure 1). For example, $d/h = 0.5$ is used in [11] (pp. 608). Here, for illustration, we adopt some overly high values of $d/h$ to examine Eq. 2.

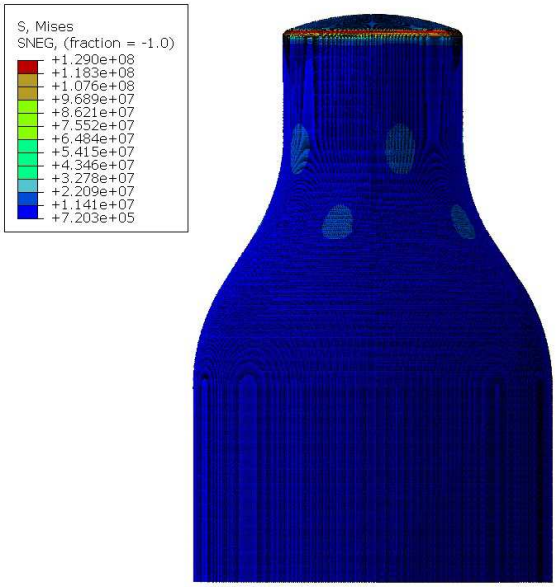


Figure 7: Results of linear stress analysis of a perturbed geometry with $d/h = 1.5$.

Results from an initial linear stress analysis on a perturbed geometry with $d/h = 1.5$ are shown in

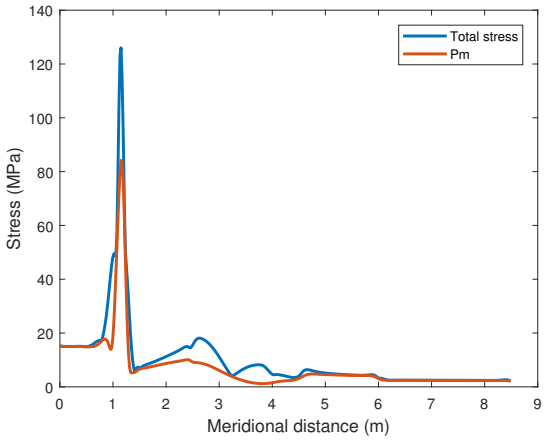


Figure 8: Membrane stresses, and total stresses (von Mises), plotted as a function of curvilinear distance measured along the shell, for $d/h = 1.5$. The oscillations in the total stress value are because of the oscillatory perturbation in shape: they are not numerical artifacts.

figure 7. A stress plot along the lines of figure 5 (left) is shown in figure 8. The perturbation in geometry has influenced stresses mainly in the buckling region. The maximum bending plus membrane stress ($S_d$) at the fillet region has remained unchanged. The maximum membrane stress $P_m$ has increased, but as explained above, to be conservative we will use the *smaller* $P_m$, i.e., from the ideal geometry or figure 5. In other words, for this structure, the effective imperfection computed using Eq. 2 is independent of the actual imperfection.

To better understand the role of $d/h$ in these calculations, we carry out several linear elastic stress calculations with

$$\frac{d}{h} = 0.5,\ 1.0,\ 1.5,\ 2.0,\ 2.5,\ \text{and}\ 3.0.$$

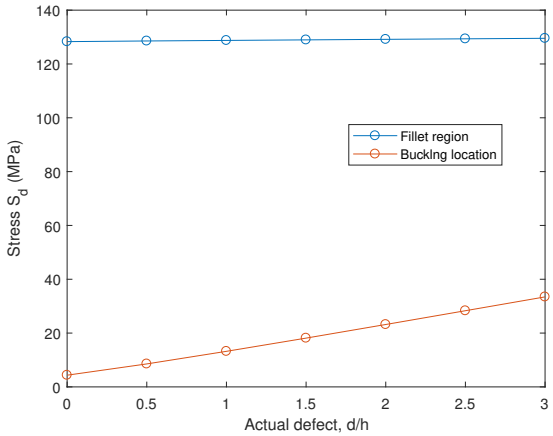


Figure 9: $S_d$ at two locations: the fillet region, and in the buckling region. The horizontal axis depicts imperfection $d/h$.

Results are summarized in figure 9. It is seen that for all values of $d/h$ any thin shell designer in the nuclear industry is likely to use, $S_d$ does not change at all; and $P_m$ is lowest for the unperturbed structure and so that, too, does not change.

Thus, for our first example, namely the nonuniform cylinder with a spherical cap, by the third method

of imperfection estimation, $d_{new}/h$ is independent of imperfection, and is in fact remarkably low (about 0.12), more than 4 times smaller than the typically used value of 0.5.

We now consider our second example.

## 4.2 Ellipsoidal head

In the ellipsoidal head, maximum stress severity occurs at approximately 100 mm below the junction between the ellipsoidal head and the cylindrical portion. Maximum displacement due to buckling occurs approximately 600 mm below that junction. Figure 10 shows the von Mises stress distribution and the first elastic buckling mode of the ellipsoidal head (displacements are exaggerated).

As before, we perturb the geometry of the ellipsoidal head with imperfections of magnitudes

$$\frac{d}{h} = 0.5,\ 1.0,\ 1.5,\ 2.0,\ 2.5,\ \text{and}\ 3.0.$$

Stress profiles are plotted for $d/h = 1.5$ in figure 11. A rather significant increase in $S_d$ is seen.

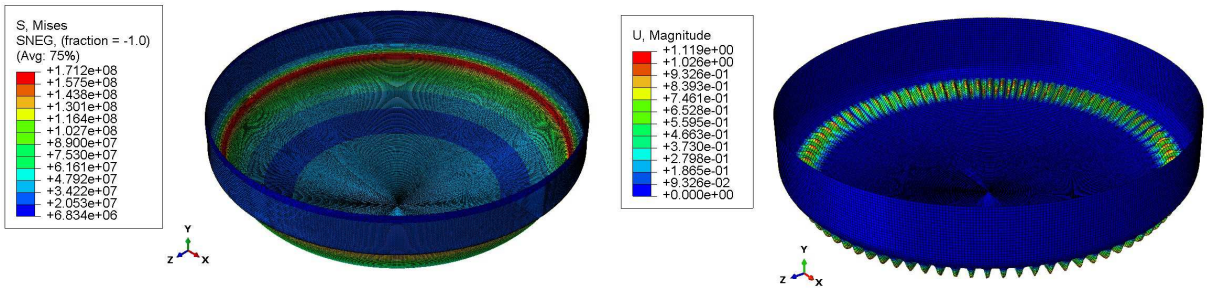


Figure 10: Ellipsoidal head. (a) von Mises stress distribution; (b) first buckling mode.

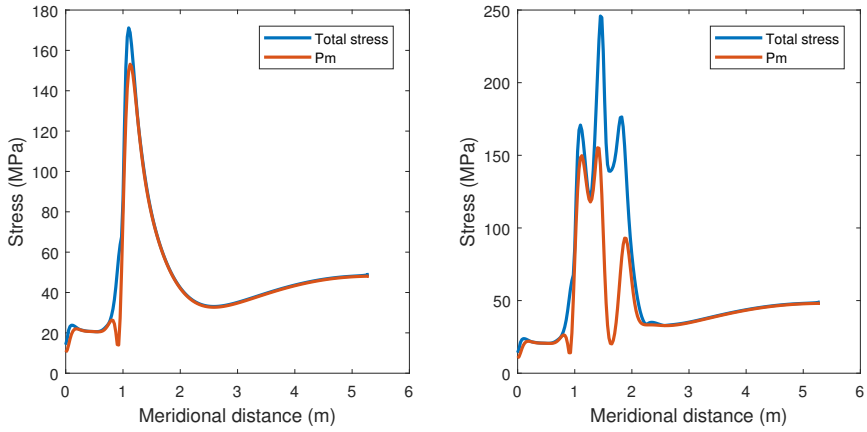


Figure 11: von Mises stress variation along the meridian of ellipsoidal head. Left: Perfect geometry. Right: geometry perturbed with imperfection $d/h = 1.5$.

Figure 12 shows the final key results for different values of $d/h$. The increase in $S_d$ notwithstanding, the computed imperfection seems too small. For the practical or reasonable value of $d/h = 0.5$, the new imperfection is about 25 times smaller at about 0.02, which is unreasonably small. In our opinion, such low imperfection is near-impossible to fabricate for large commercial thin-walled structures. For the impractically large value of $d/h = 3$, the new imperfection is about 15 times smaller at about 0.2, which is much smaller than the typical value of 0.5.

The dramatic conclusions from the study of the ellipsoidal head bear emphasis. The structure does not even have a sharp discontinuity. Yet, for an assumed physical imperfection of 0.5, Eq. 2 allows the designer to claim an imperfection that is *twenty five times smaller*, i.e., the structure can be treated as essentially perfect.

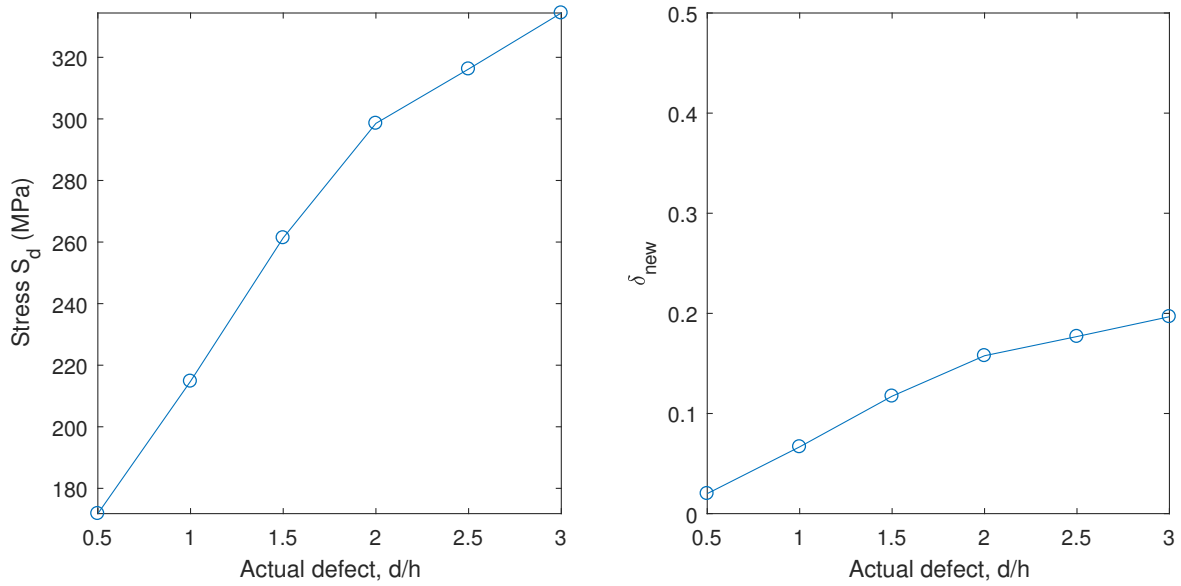


Figure 12: Ellipsoidal head. Left: Maximum stress $S_d$ against actual $d/h$. Right: Computed new defect against actual $d/h$.

We now turn to our third and final example.

### 4.3 L-shaped shell under vertical end load

Figure 13 shows the von Mises stress distribution and first buckling mode of the L-shaped shell. The maximum stress occurs at the bend. Maximum displacement due to buckling occurs at the cylinder's free edge. Note that the region near the free edge does not have the largest deformations, merely the largest displacements; but it controls the magnitude of the imperfections to be considered in the perturbed geometry. Not surprisingly, therefore, stress analysis with a perturbed geometry shows no significant amplification of the stress levels at the bend location: see figure 14, where we have used $d/h = 1.5$. Figure 15 shows the variation of maximum stress intensity $S_d$, and $d_{\text{new}}$ computed as per Eq. 2. It is seen that the computed effective imperfection as per Eq. 2 is essentially independent of the actual imperfection used, and is also extremely low (around 0.07 over a large range of actual imperfection).

The low values of new imperfection computed for all three examples in this section will result in high predictions of allowable safe loads, as we will see next.

## 5 Final safe load estimation

Having decided on the imperfection value $\delta$, and computed the eigenvalue analysis based load multiplying factor $\lambda$ for all three design cases, it remains to obtain $\zeta$ by dividing with the yield stress of the material (recall section 2). For all three cases, we will use the chart for unstable post buckling behavior (figure 1) to be conservative. We will compute safe buckling load as per both, the first method and third method of quantifying imperfections.

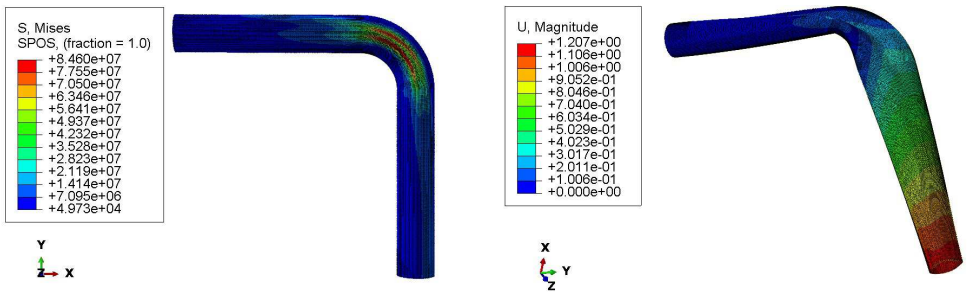


Figure 13: (a) von Mises stress distribution in L-shaped shell. (b) First buckling mode.

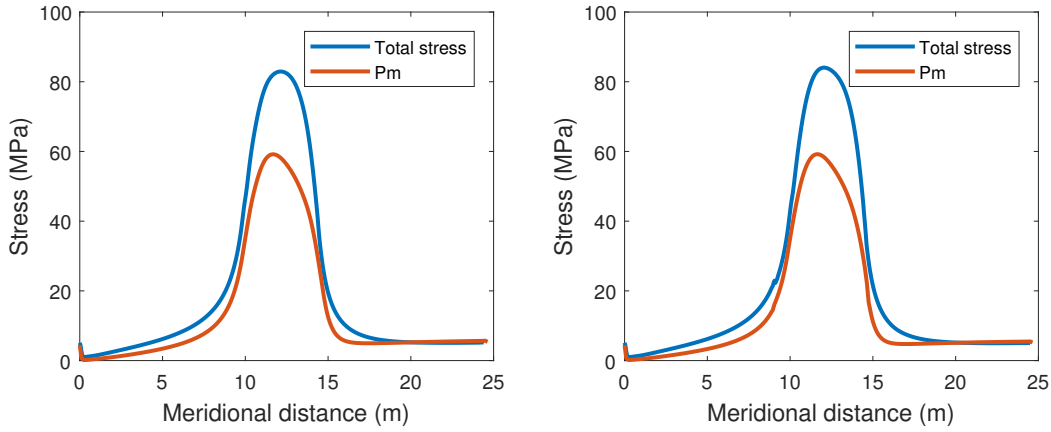


Figure 14: von Mises stress along the L-shaped shell (along different lines: one that passes through the point of maximum $S_d$ and on that passes through the point of maximim $P_m$). Left: ideal geometry. Right: perturbed geometry with $d/h = 1.5$.

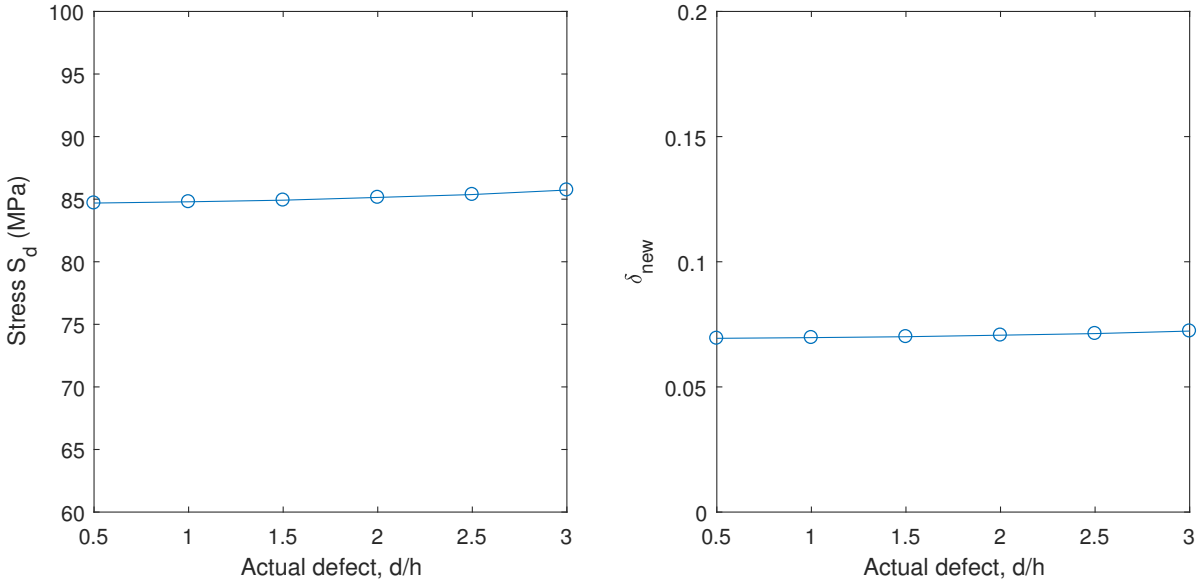


Figure 15: L-shaped shell. Left: maximum stress $S_d$. Right: new defect against actual defect.

We first compute the safe buckling load for the nonuniform cylinder with a spherical cap.

The pertinent facts from the eigenvalue analysis are as follows. The notional load is $N = 50$ KPa, and the load multiplier $\lambda = 6.8229 \approx 6.82$. The critical elastic stress, for the applied pressure 50 KPa from Fig. 5, is 83.73 MPa. The yield stress of stainless stain 316 LN at room temperature is 220 MPa [10]. We find

$$\zeta = \frac{83.73 \times 6.82}{220} = 2.5967 \approx 2.6.$$

With the first method, with $\zeta = 2.60$ and a defect of $d/h = 1.5$, from the chart, $X(\zeta, \delta) = 0.0517$, leading to a predicted safe load of 1.03 KPa. However, with the third method, with $\zeta = 2.60$, and new imperfection estimate $d_n/h \approx 0.09$, we obtain from the chart $X(\zeta, \delta) = 0.226$, leading to a predicted safe load of 4.53 KPa. In other words, a designer using Eq. 2 can claim a safe load that is about 4.4 times bigger than predicted using the standard method.

Details of similar calculations for the ellipsoidal head and the L-shaped shell are given appendix A3. Here we report the final (large) factors by which the load can be apparently multiplied within safe limits.

For the ellipsoidal head, safe buckling loads as per the first and third methods are $0.33$ KPa and $1.33$ KPa respectively, i.e., a factor of 4. For the L-shaped shell, safe end loads as per the first and third methods are $20.3$ N/m and $94.16$ N/m respectively, i.e., a factor of 4.6.

These three factors by which the safe load "increases" simply by use of Eq. 2, namely 4, 4 and 4.6, seem large. To understand the implications better, we can reconsider the calculation using a hypothetical example as follows (details not presented).

Comparing imperfection values of 1.5 (usually too high) against a claimed value of 0.07 (very low) for an SS 316 LN structure operating at 525 degrees C, with a yield stress of 107 MPa, in the first case we may be allowed a maximum stress of 6.3 MPa (impractically low) while in the second case we may be allowed a maximum stress of 30.2 MPa (with progress possible). A designer who did not have permission to use the third method of imperfection quantification would be forced to consider other, possibly more expensive or more clever, designs. A designer who was allowed to use the third method, on the other hand, would quickly settle on an easy, code-backed, and yet probably nonconservative, design option.

## 6 Three ways in which Eq. 2 can fail

We recall Eq. 2,

$$d_{new} = \frac{h}{6}\left(\frac{S_d}{P_m} - 1\right),$$

and note that the critical stresses ($S_d$, membrane plus bending; and $P_m$, membrane only) involve calculation with a notional and a perturbed geometry. The perturbation to the geometry is in the shape of the buckling mode shape, with amplitude equal to the actual physical imperfection $d$. The foregoing examples illustrate three ways in which the strategy can fail.

First, the buckling displacements may be localized to regions that are far away from the points where $S_d$ and $P_m$ are large. Subsequent perturbation in the shape of the buckling mode shape then leave the critical stress locations unaffected, and the new computed imperfection is found to be independent of the actual imperfection. This was observed in the first example (nonuniform cylinder with spherical head).

Second, even after perturbation, the ratio of $S_d/P_m$ may not be significantly greater than unity; for example, if the ratio is 1.12, say, then we have an imperfection of about 0.02, which is unrealistically small and dangerous. This could potentially happen for some shells where the ratio was close to unity to begin with. Such was observed in the second example (ellipsoidal head).

Third, although buckling occurs at some highly stressed location, due to some long unbuckled section the actual displacement may be relatively much bigger at some faraway location. On scaling the perturbation to

match the largest displacement to the physical imperfection, we then end up hardly perturbing the geometry where it most needs to be perturbed, and thereby end up with a small and insensitive imperfection value. This last possibility was observed in the third example (L-shaped shell).

# 7 Discussion and conclusions

Liquid metal cooled fast reactors must be designed to be safe under all types of loading, to the extent of our knowledge and understanding. Yet, the response of large thin shells, containing low-viscosity liquid metal, under random loading that might conceivably excite complex dynamic fluid-structure interactions and resonances, is *extremely* difficult to predict with high accuracy and confidence. This is why we use design codes, and it is critically important that the codes be conservative.

Specified limits on geometric imperfection (i.e., manufacturing tolerances) strongly influence the cost of large thin-walled shell structures. Requiring tighter tolerances raises costs significantly. Thus, a code-backed ability to claim a small imperfection value while allowing larger manufacturing tolerances lets the designer lower costs.

Additionally, for structures with unstable post buckling behavior, it is well known that the buckling load is highly imperfection sensitive [3]. In this light, the surprising observation that the effective imperfection can be independent of the actual imperfection contradicts wide experience.

Finally, a designer who finds that the safe load for his structure is both high and independent of imperfection may be tempted to lower wall thicknesses in places to reduce costs further, potentially driving up the unsafeness of the structure.

For these reasons, we suggest that the third method of imperfection estimation in RCC-MR be reconsidered carefully by its authors, if not entirely removed.

# Acknowledgements

We thank S.D Sajish, S. Jalaldeen, K. Velusamy in IGCAR for support and encouragement. AC thanks Sovan Das, Devlina Chatterjee, P. Venkitanarayanan and Anurag Gupta for useful comments.

**Data accessibility.** Available from the first author upon email request. We can upload them in the electronic supplementary material if so advised.

**Author contributions.** Ashok Kumar conducted all the finite element simulations, and contributed to the writing. Anindya Chatterjee conceived the program, participated in discussion and contributed to the writing.

**Competing interests.** The authors have none.

# References

[1] RCC-MR, Analyses taking account of Buckling, Section III-tome-1-subsection Z-Appendix A-7, 2012.

[2] B. Autrusson, D Acker, and A. Hoffmann. Discussion and validation of a simplified analysis against buckling. *Nuclear Engineering and Design*, 98:379–393, 1987.

[3] J.W Hutchinson and W.T Koiter. Postbuckling theory. *Applied Mechanics Reviews*, 23:1353–1366, 1970.

[4] G.J Simitses. Buckling and post buckling of imperfect cylindrical shells: a review. *Applied Mechanics Reviews*, 39:1517–1524, 1986.

[5] J.G Teng. Buckling of thin shells: recent advances and trends. *Applied Mechanics Reviews*, 49:263–274, 1996.

[6] Jian Zhang, Meng Zhang, Wenxian Tang, Weibo Wang, and Minglu Wang. Buckling of spherical shells subjected to external pressure: A comparison of experimental and theoretical data. *Thin-Walled Structures*, 111:58 – 64, 2017.

[7] M. Tall, S. Hariri, P. Le Grognec, and Y. Simonet. Elastoplastic buckling and collapse of spherical shells under combined loadings. *Thin-Walled Structures*, 123:114 – 125, 2018.

[8] O. Ifayefunmi. Buckling behavior of axially compressed cylindrical shells: Comparison of theoretical and experimental data. *Thin-Walled Structures*, 98:558 – 564, 2016.

[9] Yongmei Zhu, Yongjian Dai, Qingli Ma, and Wenxian Tang. Buckling of externally pressurized cylindrical shell: A comparison of theoretical and experimental data. *Thin-Walled Structures*, 129:309 – 316, 2018.

[10] Properties groups for materials, Section III-tome-1-subsection Z-Appendix A-3, 2012.

[11] B Raj, P. Chellapandi, and P.V. Rao. *Sodium fast reactors with closed fuel cycle*. CRC Press, 2015.

# Appendix

## A1 $P_m$ and $P_m + P_b$ calculation

Procedures summarized here (for completeness) are based on *RCC-MR Section III Tome 1 Subsection B*. First the membrane stress tensor is computed from the mean values of individual stress components $\sigma_{ij}$ averaged across shell thickness (*RB 3224.12, pp. 25*),

$$(\sigma_{ij})_m = \frac{1}{h}\int_{-h/2}^{h/2} \sigma_{ij} dx \tag{A1.1}$$

where $h$ is the shell thickness and $x$ is a local through-thickness integration variable. Similarly, the bending stress tensor is calculated from the total stress tensor components, each averaged by integration *RB 3224.13 (page number 25)* as in

$$(\sigma_{ij})_b = \frac{12x}{h^3}\int_{-h/2}^{h/2} \sigma_{ij} x dx. \tag{A1.2}$$

The equivalent stress or stress intensity for a given stress tensor with principal stresses $\sigma_1$, $\sigma_2$ and $\sigma_3$ is given as per *RB 3224.43 (page number 27)* by

$$\bar{\sigma} = \sqrt{\frac{(\sigma_1 - \sigma_2)^2 + (\sigma_1 - \sigma_3)^2 + (\sigma_3 - \sigma_2)^2}{2}}. \tag{A1.3}$$

As per *RB 3224.51*, primary membrane stress intensity $P_m$ is calculated from principal stresses of the membrane stress tensor (A1.3). To calculate $P_m + P_b$, first a membrane plus bending stress tensor is constructed by adding

$$(\sigma_{ij})_{m+b} = (\sigma_{ij})_m + (\sigma_{ij})_b$$

and then the $P_m + P_b$ stress intensity is calculated as per (A1.3) from principal stresses of the above $(\sigma_{ij})_{m+b}$.

## A2 Mesh convergence studies

In mesh convergence studies, successive mesh models are created by halving the element sizes of previous mesh models.

For the nonuniform cylinder with a spherical cap, the initial mesh model used had an element size (h) of 160 mm, and successive meshes had element sizes of 80 mm, 40 mm, 20 mm and 10 mm. For the elliptical head with cylinder, the initial mesh model used had an element size of 400 mm, and then successive models had element sizes of 200 mm, 100 mm, 50 mm and 25 mm. For the L-shaped pipe, the initial mesh model had an element size of 200 mm, with subsequent meshes of 100 mm, 50 mm and 25 mm.

Two solution quantities, namely the stress at a critical location in the model and the total strain energy, were used to study convergence for the different models. Both parameters are plotted against $1/h$ (with $h$ in mm).

Figures 16, 17 and figure 18 show that good convergence was obtained with the element sizes finally used. The percentage changes observed due to the final refinement steps were tiny in all three cases.

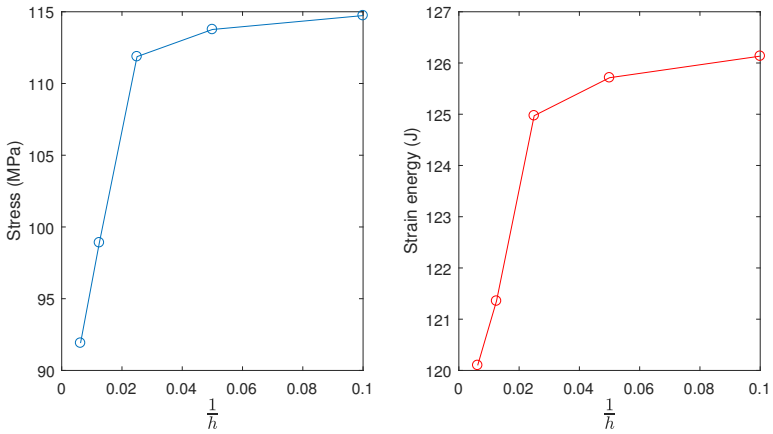


Figure 16: Mesh convergence for the nonuniform cylinder with spherical cap. (a) von Mises stress, (b) strain energy.

## A3 Safe buckling load calculation details

In this section, we present some safe load calculation details for the ellipsoidal head and the L-shaped shell. It will be seen that, except for our use of Eq. 2, we have been conservative in all other ways.

### A3.1 Ellipsoidal head

For the ellipsoidal head, the notional load is $N = 15$ KPa. The location of maximum membrane plus bending stress is not at structural discontinuity. See figure 11. Hence we shall compute the safe buckling

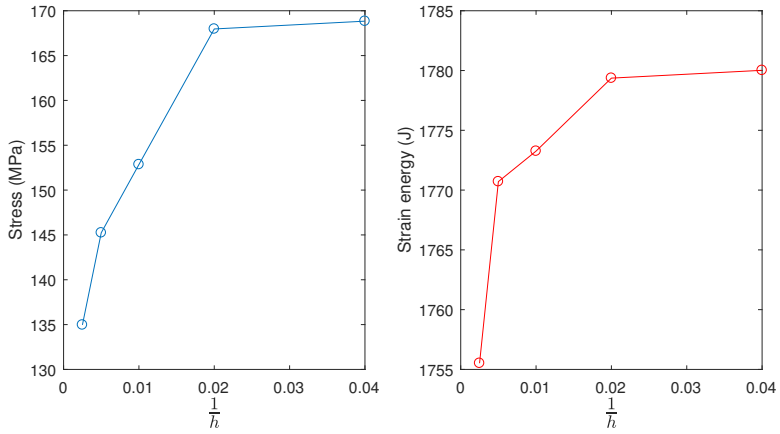


Figure 17: Mesh convergence for the ellipsoidal head. (a) von Mises stress, (b) strain energy.

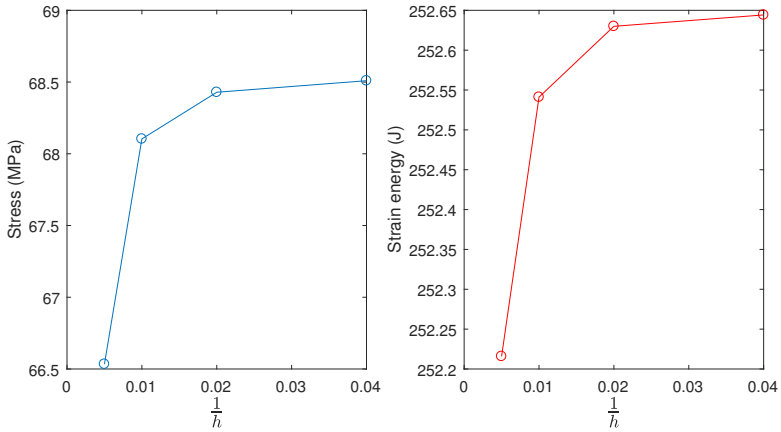


Figure 18: Mesh convergence for the L-shaped pipe. (a) von Mises stress, (b) strain energy.

load using both, just the membrane $P_m$ stress intensity as well as the membrane plus bending $(P_m + P_b)$ stress intensity. We shall take the lower permissible load obtained as the safe load.

We will denote the $\zeta$ due to membrane $P_m$ stress intensity as $\zeta_m$, and denote the $\zeta$ due to membrane plus bending $(P_m + P_b)$ stresses intensity as $\zeta_{m+b}$.

From linear stress analysis, as shown in figure 11, $P_m$ is 153.4 MPa and $P_m + P_b$ is 171.25 MPa. From linear buckling analysis, the load multiplier $\lambda = 3.45$. We obtain

$$\zeta_m = \frac{153.4 \times 3.45}{220} \approx 2.41$$

and

$$\zeta_{m+b} = \frac{171.25 \times 3.45}{220} \approx 2.69$$

First let us consider membrane stress intensity alone. For actual defect $d/h = 1.5$, we obtain from charts $X_m(\zeta, \delta) = 0.0552$. For the equivalent new defect $d/h = 0.1173$, we obtain $X_m(\zeta, \delta) = 0.2225$. The safe buckling load as per the first and third methods are $0.33$ KPa and $1.33$ KPa respectively.

Now we consider both membrane and bending stress intensity. For actual defect $d/h = 1.5$ and $\zeta_{m+b} = 2.69$, we obtain from the chart $X_{m+b}(\zeta, \delta) = 0.0503$. For the equivalent new defect $d/h = 0.1173$, we obtain from the chart $X_{m+b}(\zeta, \delta) = 0.2043$. The safe buckling load as per first and third method are $0.45$ KPa and $1.84$ KPa respectively.

To be conservative, we adopt the first estimates as the safe loads.

## A3.2 L-shaped shell

For the L-shaped shell, the notional load is $N = 1000$ N/m, and the load multiplier $\lambda = 9.78$.

From linear stress analysis, as shown in figure 14, $P_m$ is 59.59 MPa and $P_m + P_b$ is 84.6 MPa. Accordingly,

$$\zeta_m = \frac{59.79 \times 9.78}{220} \approx 2.66$$

and

$$\zeta_{m+b} = \frac{84.6 \times 9.78}{220} \approx 3.76$$

From the charts, for an actual defect $d/h = 1.5$ and $\zeta_m = 2.66$, we obtain $X_m(\zeta, \delta) = 0.0507$. For the equivalent new defect $d/h = 0.07$, we obtain $X_m(\zeta, \delta) = 0.2354$. The safe buckling load as per first and third methods are $20.3$ N/m and $94.16$ N/m.

Similarly, for $d/h = 1.5$ and $\zeta_{m+b} = 3.76$, we obtain from the chart $X_{m+b}(\zeta, \delta) = 0.0378$. For the equivalent new defect $d/h = 0.07$, we obtain from the chart $X_{m+b}(\zeta, \delta) = 0.1791$. The safe buckling loads as per the first and third methods are $22.65$ N/m and $107.43$ N/m respectively.

To be conservative, we again adopt the first set of values.